Electron density of (1 × 2)Pt(110) from He reflectivity measurements

D. Cvetko,* V. De Renzi,† L. Floreano,‡ A. Lausi,§ A. Morgante, M. Peloi, and F. Tommasini‡
Laboratorio INFM-TASC, Padriciano 99, 34012 Trieste, Italy

E. Kirsten and K.H. Rieder
Freie Universität Berlin, Arnimallee 14, 14195 Berlin, Germany
(Received 17 November 1994)

The electron density of the (1 × 2)Pt(110) surface is determined by He reflectivity measurements and compared to the electron densities previously reported for (1 × 2)Au(110) and (1 × 2)Rh(110). With respect to the superposition of free atomic electron densities, significant charge depletion and enrichment are observed, respectively, *on top* of the surface atoms and in the threefold sites of the (111) microfacets.

I. INTRODUCTION

He beam scattering from solid surfaces is known to be a powerful tool for the study of surface structures[1,2] and vibrations[3,4] and allows studies of surface phase transitions,[5] crystal growth[6] and nonequilibrium phase evolution[6–8] to be performed in an extended range of surface temperatures. The most specific feature of the He probe is that it samples the valence charge distribution at the surface, in contrast with probes such as electrons and x rays, which mainly detect the core electron densities. Moreover, He atoms are not expected to perturb the valence electron density, while this is hardly the case for tunneling microscopy.

Experimentally, it is easy to determine the shape of the He-surface interaction potential on metallic surfaces with relatively low corrugation by measuring the He diffraction patterns and the He bound state resonances.[9] The diffraction intensities, modulated by surface rainbow effects arising from the corrugation of the repulsive wall, reveal the variation of the He turning point along the surface and, therefore, reflect directly the corrugation of the relevant surface electron density,[10] while the bound state spectrum allows the laterally averaged well bottom to be properly described.

On highly corrugated surfaces, like (1×2)-missing-row-reconstructed Au(110) and Pt(110), the identification of the bound state features in the scattering patterns is by no means simple, however, on (1 × 2)Pt(110) the main features have been identified and a model potential in agreement with scattering data has been reported.[11,12] This model is highly satisfactory as far as the effective corrugation of the repulsive wall and the laterally averaged well bottom are concerned, nevertheless it does not account for the lateral modulation of the potential well depth.

Recently, it has been demonstrated that measurements of the specular reflectivity of a low-energy He beam at grazing incidence from highly corrugated surfaces[2,13] contain an astonishing amount of information on the He-surface interaction potential and on the surface electron density.[13] The reason for this is that He atoms at grazing incidence have quite long collision times since multiple reflections at the repulsive and attractive walls take place for most of the collision paths and the phase shifts of the outgoing He waves depend dramatically upon the specific path. As a consequence, the well bottom region of the potential is quite accurately explored and the lateral modulations of the well depth become detectable.

In the present paper, we report He-reflectivity measurements for (1 × 2)Pt(110) and analyze the data by the method previously used for the (1 × 2)Au(110) surface. Pt and Au crystals have quite similar lattice parameters (3.92 Å and 4.08 Å, respectively) and for both of them, the (110) surface reconstructs at low temperatures in a (1 × 2)-missing-row structure, where every second row in the [001] direction is missing. Maps of the surface electron density show an evident lateral spread of the electron charge with respect to the superposition of unperturbed atomic electron densities. While this is a nonsurprising result for metals,[14] the fact that the He-reflectivity method measures the extent of such spreads is quite satisfactory. Since the electron densities of free Pt and Au atoms are almost exactly the same in the whole region explored by He atoms,[15] the issue of whether the atomic densities are spread at the surface in different ways as a consequence of the different electronic configurations in the solid is of current interest.

II. EXPERIMENT

The He-beam apparatus is described in detail elsewhere.[16] Both the beam source and the detector are fixed at an angle of 110° and their axes define the scattering plane. The Pt crystal is cut along the (110) surface within 0.2° and is mounted on a manipulator with six degrees of freedom, accurate to within a few μm and within 0.01°, respectively, for translations and rotations. This allows the incidence angle Θ_i, the tilt angle Δ, and the azimuthal angle ϕ to be selected. Θ_i and Δ are the angles formed by the surface normal with the beam axis

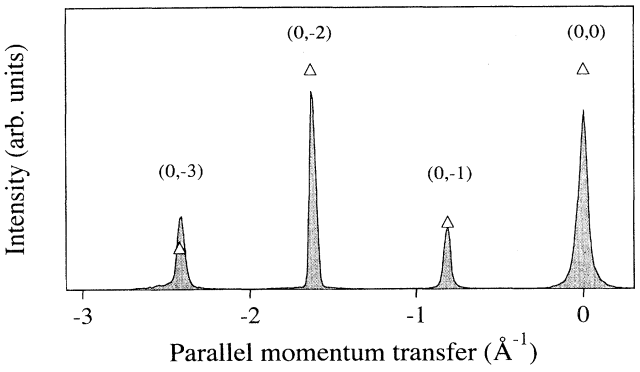

FIG. 1. The (1 × 2)Pt(110) diffraction pattern taken with a beam energy of 19.0 meV (wave vector $k = 6.06$ Å^{-1}) along the ΓY ($\phi = 0°$) direction. The open triangles (△) are the calculated intensities.

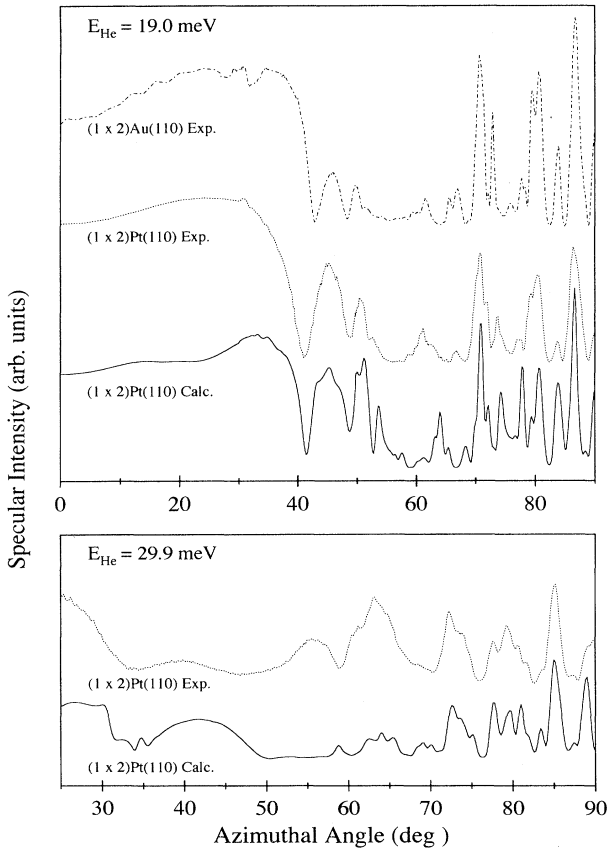

FIG. 2. Upper panel: He specular reflectivity measurements $I(\phi)$ for (1×2)Au(110) (dashed line), and (1×2)Pt(110) (dotted line) taken with the energy of 19.0 meV. Calculated specular reflectivity is also presented (full line). Lower panel: He specular reflectivity measurements $I(\phi)$ for (1 × 2)Pt(110) (dotted line) and calculated reflectivity (full line) taken with the energy of 29.9 meV.

and with the scattering plane, respectively, while ϕ is the angle formed by the [001] (ΓY) surface direction (perpendicular to the rows of close-packed Pt atoms) and the scattering plane. All measurements are taken by detecting time of flight (TOF) distributions of the scattering intensities and by selecting the count rates in an energy window of ±0.3 meV, centered at the TOF elastic peak. The He beam energy may be selected in the range between 19–70 meV by varying the He source temperature. For the lowest beam energies a relative velocity spread $\frac{\Delta v}{v}$ of 1.1% is reached. This allows the transfer width of the apparatus to exceed 1200 Å.

The Pt crystal was polished and kept in a hydrogen atmosphere at 1300 K for 72 h. It was then additionally cleaned in vacuum by Ar^+ ion bombardment (1–3 keV) and annealing to 1300 K. Repeated oxidation-reduction cycles at 1000 K also improved the surface quality and eventually a clean and well-ordered missing row structure was obtained. The (1 × 2)Pt(110) diffraction pattern taken with a beam energy of 19.0 meV (wave vector $k = 6.06$ Å^{-1}) along the ΓY ($\phi = 0°$) direction is shown in Fig. 1. In the ΓX ($\phi = 90°$) direction the diffraction pattern shows very weak first-order diffracted peaks with intensity of 2.6×10^3 times lower than the specular one. For this particular beam energy, the waves scattered in the specular direction (momentum exchange $\Delta k_\perp = 6.95$ Å^{-1}) from surface terraces separated by monoatomic steps ($\Delta h = 1.38$ Å) are closely in antiphase conditions ($\Delta k_\perp \Delta h = 3.05\pi$). As a consequence, the angular width of the specular peak reflects the distribution of surface terraces. In particular, the average distance between flat terraces has been evaluated from the specular peak widths to be 800 Å and 300 Å, respectively, along the [1$\bar{1}$0] and [001] surface directions.

In Fig. 2, He specular reflectivity measurements $I(\phi)$ are reported as a function of the azimuthal orientation, with the beam energy of 19.0 and 29.9 meV (wave vector $k = 7.68$ Å^{-1}), respectively, for the upper and lower panel. For both beam energies the spectra show numerous structures caused by the multiple scattering in the three-dimensional He-surface potential. For comparison, we also show the very similar $I(\phi)$ curve previously taken for the (1 × 2)Au(110) surface[2] with the same beam energy.

III. ANALYSIS

The analysis of the He-reflectivity measurements for (1 × 2)Au(110) and (1 × 2)Rh(110) was previously performed[2,13] by modeling the He-surface interaction potential as a superposition of pseudopair anisotropic terms given by

$$v(\mathbf{r}) = \eta_x\eta_y v\left(\sqrt{z^2 + (\eta_x x)^2 + (\eta_y y)^2}\right), \qquad (1)$$

where η_x and η_y are anisotropy parameters and the function $v(r)$ is chosen according to the available models for the van der Waals pair potentials.[17,18] Close-coupled-channels calculations (CCC) of the scattering probabili-

ties were then performed for the superposition of pseudopair terms and compared to the scattering intensities. Here, we follow the same procedure with minor changes suggested by a recent study of van der Waals pair potentials.[15] It has been shown that, for noble atom–metal atom pairs, the function

$$u(r) = \frac{C_6}{120}\left(\frac{b}{3}\right)^6 (ae^{-br} - 84e^{-2br/3} - e^{-br/3}) \quad (2)$$

fully describes the pair potential in a wide range of internuclear separations extending well beyond the inflection point. Moreover, the range parameter b is related to the unperturbed electron densities of the two atoms; if these decay with distance with logarithmic slopes β_1 and β_2, then b is given by

$$\frac{1}{b^3} = \frac{1}{\beta_1^3} + \frac{1}{\beta_2^3}. \quad (3)$$

Therefore, when the dipole-dipole coefficient C_6 is known, a is the only free parameter entering the pair potential. A correction to $u(r)$ is required at very long range in order to reproduce the asymptotic behavior C_6/r^6. However, when the superposition of pair potentials is considered, the long range correction does not affect the periodic Fourier components and only gives a contribution $W(z)$ to the laterally averaged atom-surface potential.[2] This contribution approaches the Zaremba and Kohn dispersion energy[19] at long range and is given by

TABLE I. Parameters of the interaction potential for a few He-metal systems.

	C meV Å^3	b Å^{-1}	a	η_x	η_y	Ref.
(1 × 2)Au(110)	275	2.55	2400	0.81	0.81	29
(1 × 2)Pt(110)	308	2.55	2350	0.78	0.78	
(1 × 2)Rh(110)	274	2.57	2230	0.83	0.74	13

$$W(z) = -\frac{C}{(z-z_0)^3 + (17/b)^3 e^{-\frac{1}{4}(\frac{b(z-z_0)}{17})^3}}, \quad (4)$$

where the atom-surface dispersion coefficient C is related to C_6 and to the atomic volume Ω in the solid as

$$C_6 = \frac{6\Omega C}{\pi}, \quad (5)$$

and z_0 is the position of the image plane with respect to the outermost nuclear plane.[19] The superposition of pseudopair anisotropic terms $u(\mathbf{r})$ with the correction $W(z)$ given by Eq. (4) is then used to model the interaction of helium atoms with solid surfaces. For (1 × 2)Au(110) and (1 × 2)Rh(110) the present model, with parameters set as given in Table I, leads to the potentials equivalent to those previously reported,[2,13] except for rigid displacements along the surface normal, which do not exceed 0.1 Å and leave the quality of the previously reported fits unaltered.

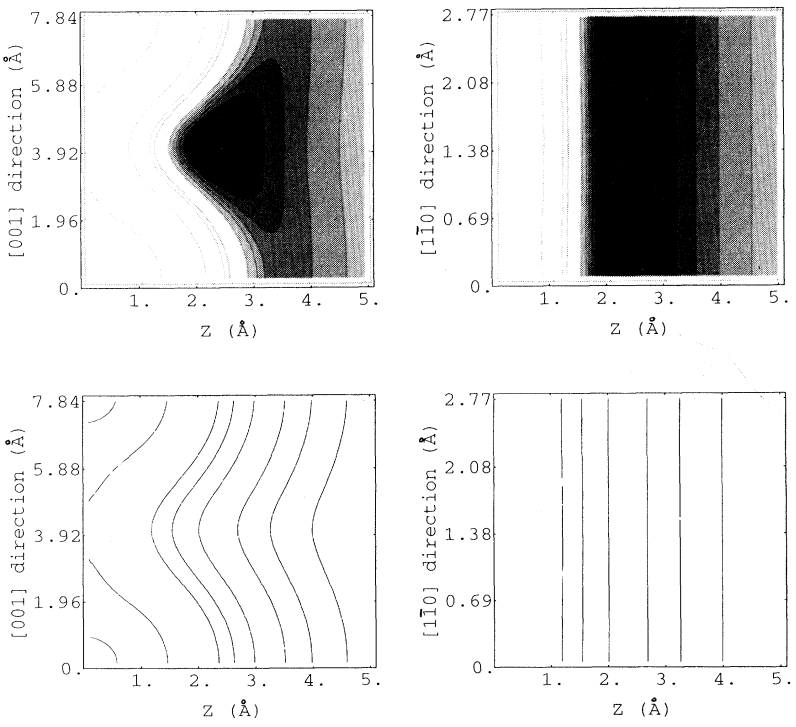

FIG. 3. Upper panel: Equipotential contour levels for the He-(1×2)Pt(110) potential drawn in the $(z, y; x = 0)$ and $(z, x; y = 3.92$ Å) planes. x, y, and z refer, respectively, to the [1$\bar{1}$0], [001], and [110] lattice direction. The potential depth is visualized by the darkness of the shaded area. The contour lines represent the equipotential levels of −14, −10, −8, −6, −4, 0, 20, 30, 100, and 1000 (this level only in zy plane) meV, respectively. Lower panel: Maps of surface electron density in the same planes of the upper panel. The contour lines correspond, respectively (from right to left), to the electron densities of 10^{-5}, 5×10^{-5}, 1.7×10^{-4}, 6.7×10^{-4}, 1.7×10^{-3}, 3.3×10^{-3}, and 3.3×10^{-2}, 0.33 (the last two levels only in zy plane) electrons Å^{-3}.

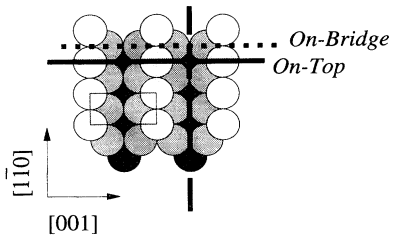

FIG. 4. Top view of the (1 × 2)-missing-row structure of Pt(110). The three lines (full, dotted and dashed) denote the directions along which the scans of Fig. 3 and Fig. 5 are taken.

The analysis of the measurements reported in Sec. II is carried out by assuming that the (1 × 2)Pt(110) surface has the structure of the (1 × 2)Au(110) surface as determined by Moritz and Wolf,[20] and scaled by slightly different lattice parameter. That the detailed structure of Pt(110) surface may be quite similar to that of Au(110) has been reported by several theoretical studies, most notably by Brocksch and Bennemann,[21] Daw,[22] and Foiles.[23] Furthermore, the choice of 20% inward relaxation of Pt topmost layer agrees also with the Fenter and Gustafsson's structural analysis by medium-energy ion scattering.[24]

Since the electron densities $n(r)$ of free Pt and Au atoms coincide within the errors in the whole range of distances where $n(r) \leq 10^{-2}$ atomic units,[25] which exceeds by far the range explored by He scattering, we set the He-Pt pair potential parameters b and C_6 equal to those of the He-Au pair. Only the parameters a, η_x, and η_y are then varied to fit the experimental data.

We start by calculating the probabilities of specular reflection for different azimuthal orientations in order to reproduce the $I(\phi)$ curve taken with 19.0 meV beam energy. The quality of the obtained fit is measured by the reliability factor[2] R_{mos}. In our case it is seen that the parameter η_x does not affect the calculated curves so we set $\eta_x = \eta_y$ and vary a and η_y in order to minimize the R_{mos}. This leads to the quite satisfactory fit shown in Fig. 2 and determines the parameters as $a = 2350 \pm 10$ and $\eta_y = 0.78 \pm 0.01$.

It is highly satisfactory that the same set of parameters accounts for the whole set of measurements. The diffraction intensities along [1$\bar{1}$0] are reproduced as shown in Fig. 1 and also the first-order diffraction peak intensity along the [001] is consistent with the choice $\eta_x = 0.78$. Furthermore, the $I(\phi)$ curve taken with 29.9 meV beam energy is reproduced accurately, as shown in Fig. 2. This firmly supports the model potential and the choice of the parameters given in Table I.

Equipotential contours for the He-(1 × 2)Pt(110) potential drawn in planes perpendicular to the surface are presented in Fig. 3 upper panel where the shaded regions refer to negative energies. The contours shown on the right-hand side, drawn above a row of missing atoms (dashed line on Fig. 4), present quite low corrugations

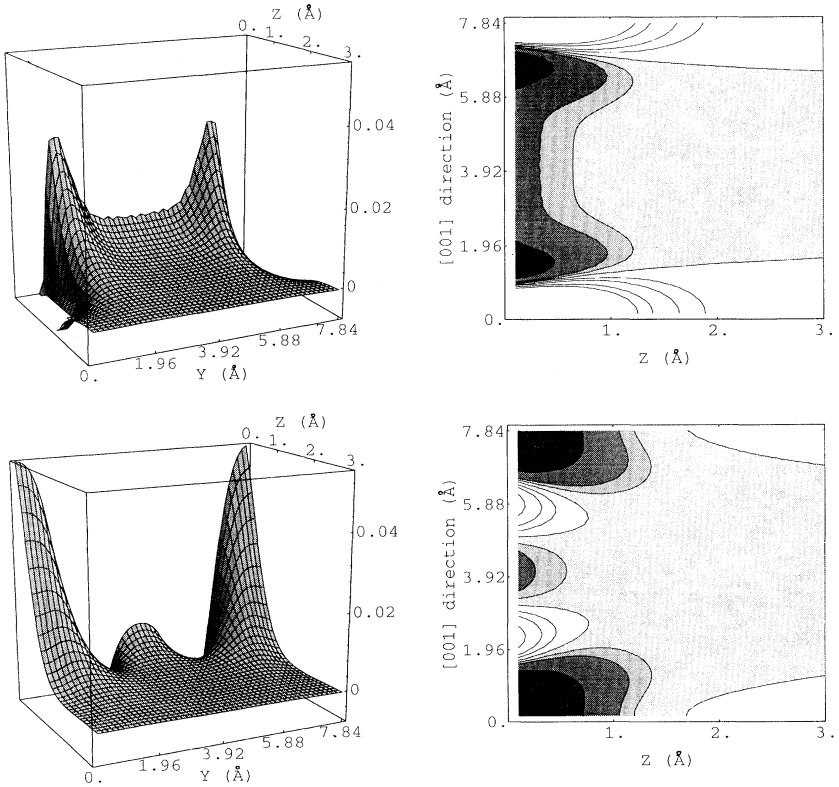

FIG. 5. Difference, $\Delta n(z, y; x = \text{const})$, between the superposition of pseudoatomic electron densities $n(\mathbf{r})$ for $\eta_x = \eta_y = 0.78$ and the superposition of free atomic densities $n(r)$, presented in the 3D figure (left-hand side) and the corresponding yz contour plot (right-hand side). x, y, and z refer, respectively, to the [1$\bar{1}$0], [001], and [110] lattice directions. The dashed region refers to the positive values of Δn. The planes considered in the upper and lower panels intersect the atomic rows, respectively, at the *on-top* ($x = 0$) and *on-bridge* ($x = 1.38$ Å) position.

and a structureless well bottom reaching −14.93 meV. In planes perpendicular to the rows (full line on Fig. 4) on the other hand, the contours are highly corrugated, as shown in the left-hand side of the same figure. In this case the 20 meV equipotential contour, which corresponds to the classical turning points, exhibits a peak-to-valley corrugation of 1.37 Å.[26]

IV. DISCUSSION

In Table I, it is shown that different metals have quite similar potential parameters, in particular in all cases the anisotropy parameters are close to 0.8 and only minor differences are observed for the parameter a. This is quite promising since it allows the interaction of He with different metal surfaces to be predicted with good accuracy by starting from the electron density of the free metal atom. In fact, according to Eq. (1), we assume that the electron density at the surface, as seen by the He atoms, may be obtained by the superposition of pseudoatomic densities,

$$n(\mathbf{r}) = \eta_x \eta_y n\left(\sqrt{z^2 + (\eta_x x)^2 + (\eta_y y)^2}\right). \tag{6}$$

With respect to the standard approach based on the Esbjerg and Nørskov approximation,[27,28,12] the present one is to be preferred since the repulsive potential wall is explored by the He atoms at low energies, where its slope is highly affected by the dispersion energy. The surface electron density contours[30] are plotted in Fig. 5 lower panel in the same planes as considered in the upper panel. It may be noted that at large separations, where the equipotential contours are essentially flat, the electron density is still quite corrugated.

In order to visualize the lateral spread of the electron charge in the surface plane, we compare the superposition of pseudoatomic densities $n(\mathbf{r})$ for $\eta_x = \eta_y = 0.78$ to the superposition of free atomic densities $n(r)$. The difference between the two superpositions is shown in Fig. 5. The planes considered in the upper and lower panels are both perpendicular to the surface and to the $[1\bar{1}0]$ atomic rows, but intersect them at the *on-top* and *on-bridge* position, respectively (see Fig. 4). It may be observed that *on top* of the surface atoms the electron density is depleted with respect to the superposition of free atomic densities (bright regions in the figures), while the reverse occurs for *on-bridge* positions. In particular, the largest charge enrichments are observed above the threefold sites of the (111) microfacets.

V. CONCLUSIONS

In conclusion, we have demonstrated that the He-reflectivity measurements on (1 × 2)Pt(110) reveal very accurately the He-surface interaction potential shape. In particular, we show that along the [001] surface direction the attraction well is strongly modulated, reaching a minimum of −14.93 meV in the trough between the Pt top-most atoms. The electron density map of the surface unit cell is found substantially more corrugated than the total interaction potential. Finally, by comparing the reflectivity measurements taken on Pt(110) and Au(110) we conclude that, even though the two surfaces have quite different electronic band structures, the electron density and the shape of the potential well, as seen by the He atom, are practically identical. This means that the geometric superposition of free atom charge densities describes quite accurately the surface electron density relevant for He-surface interaction, whereas minor deviations due to the particular solid environment may be well accounted for by the anisotropy parameters η. This confirms firmly our construction of the interaction potential and also the pairwise summation of anisotropic free atom electron densities. The region of maximum degree of charge depletion with respect to the conventional superposition is found to be most pronounced in the surface zone of low atomic density, i.e., in the threefold sites of the (111) microfacets of the Pt missing-row structure.

ACKNOWLEDGMENTS

E.K. gratefully acknowledges financial support of this work from the Deutsche Forschungsgemeinschaft via Sonderforschungsbereich 290 (Berlin). He also thanks all members of the Laboratorio TASC (Trieste) for a very fruitful stay. Helpful discussions with Professor J.P. Toennies (Goettingen) are gratefully acknowledged.

* Also at J. Stefan Institute, University of Ljubljana, Ljubljana, Slovenia.
† Also at Dipartimento di Fisica, Università di Modena, Modena, Italy.
‡ Also at Dipartimento di Fisica, Università di Trieste, Trieste, Italy.
§ Permanent address: Sincrotrone Trieste, Trieste, Italy.

[1] T. Engel and K.H. Rieder, *Structural Studies of Surfaces*, Springer Tracts in Modern Physics Vol. 91 (Springer, Berlin, 1982).
[2] P. Cortona, M.G. Dondi, D. Cvetko, A. Lausi, A. Morgante, K.C. Prince, and F. Tommasini, Phys. Rev. B **47**, 6705 (1993).
[3] J.P. Toennies, in *Dynamics of Gas-Surface Interactions*, edited by G. Benedek and U. Valbusa, Springer Series in Chemical Physics Vol. 21 (Springer, Berlin, 1982), p. 208.
[4] G. Bracco, R. Tatarek, F. Tommasini, U. Linke, and M. Persson, Phys. Rev. B **36**, 2928 (1987).
[5] A.F. Bellman, D. Cvetko, A. Morgante, M. Polli, F. Tommasini, K.C. Prince, and R. Rosei, Surf. Sci. Lett. **281**, L321 (1993).
[6] G. Comsa and B. Poelsema, *Scattering of Thermal Energy Atoms from Disordered Surfaces*, Springer Tracts in Modern Physics Vol. 115 (Springer, Berlin, 1989).

[7] D. Cvetko, A. Lausi, A. Morgante, F. Tommasini, and K.C. Prince, Surf. Sci. **269/270**, 68 (1992).
[8] J. Lapujoulade, Surf. Sci. Rep. **20**, 191 (1994).
[9] A.F. Bellman, D. Cvetko, A. Morgante, M. Polli, F. Tommasini, V.R. Dhanak, A. Lausi, K.C. Prince, and R. Rosei, Surf. Sci. **282**, 273 (1993).
[10] K.H. Rieder, in *Helium Atom Scattering from Surfaces*, edited by E. Hulpke, Springer Series in Surface Sciences Vol. 27 (Springer, Berlin, 1992), p. 41.
[11] E. Kirsten and K.H. Rieder, Surf. Sci. Lett. **222**, L837 (1989); Surf. Sci. **265**, 67 (1992).
[12] E. Kirsten, G. Parschau, and K.H. Rieder, Surf. Sci. Lett. **236**, L365 (1990).
[13] A.F. Bellman, A. Morgante, M. Polli, F. Tommasini, D. Cvetko, V.R. Dhanak, A. Lausi, K.C. Prince, and R. Rosei, Surf. Sci. **298**, 1 (1993).
[14] J. Harris and A. Liebsch, J. Phys. C **15**, 2275 (1982).
[15] D. Cvetko, A. Lausi, A. Morgante, F. Tommasini, P. Cortona, and M.G. Dondi, J. Chem. Phys. **100**, 2052 (1994).
[16] D. Cvetko, A. Lausi, A. Morgante, F. Tommasini, K.C. Prince, and M. Sastry, Meas. Sci. Technol. **3**, 997 (1992).
[17] K.T. Tang and J.P. Toennies, J. Chem. Phys. **80**, 3726 (1984).
[18] C. Douketis, G. Scoles, S. Marchetti, M. Zen, and A. J. Thakk, J. Chem. Phys. **76**, 3057 (1982)
[19] E. Zaremba and W. Kohn, Phys. Rev. B **13**, 2770 (1976).
[20] W. Moritz and D. Wolf, Surf. Sci. **163**, L655 (1985).
[21] H.-J. Brocksch and K.H. Bennemann, Surf. Sci. **161**, 321 (1985).
[22] M.S. Daw, Surf. Sci. **166**, L161 (1986).
[23] S.M. Foiles, Surf. Sci. **191**, L779 (1987).
[24] P. Fenter and T. Gustafsson, Phys. Rev. B **38**, 10 197 (1988).
[25] P. Cortona (private communications).
[26] The peak-to-valley corrugation for different He energies varies slightly, e.g., it reaches 1.44 and 1.39 Å for 0 and 100 meV, respectively.
[27] N. Esbjerg and J.K. Nørskov, Phys. Rev. Lett. **45**, 807 (1980).
[28] M. Manninen, J.K. Nørskov, M.J. Puskar, and C. Umrigar, Phys. Rev. B **29**, 2314 (1984).
[29] D. Cvetko, V. De Renzi, L. Floreano, R. Gotter, A. Morgante, M. Peloi, F. Tommasini, C. Mannori, and M.G. Dondi (unpublished).
[30] The surface electron density is obtained from the repulsive part of the total He-surface potential as $n(\mathbf{r}) = \alpha^{-1} V_{\mathrm{rep}}(\mathbf{r})$ with $\alpha = 30$ eV Å^3 after Ref. 28.

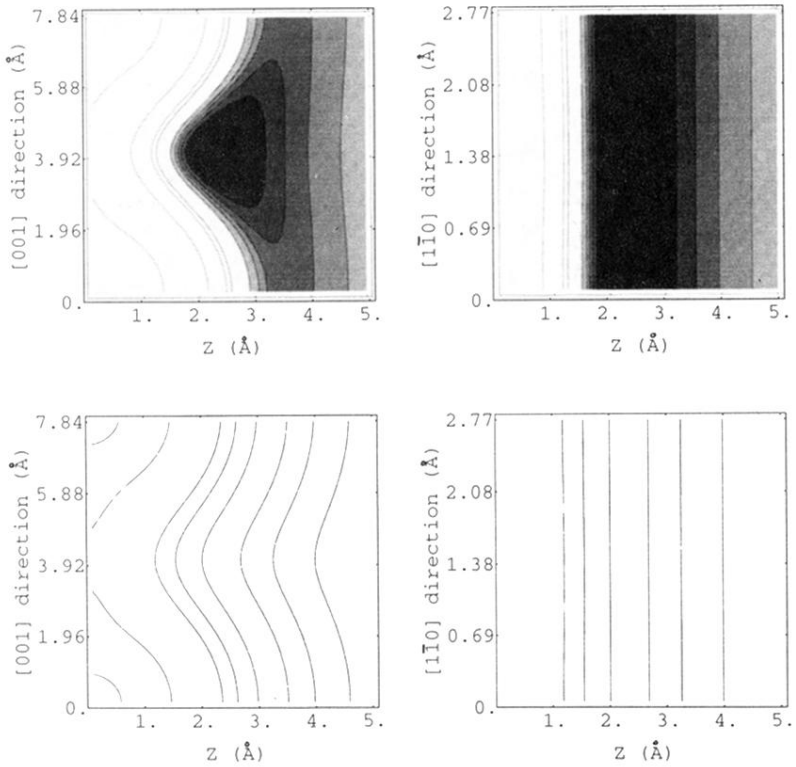

FIG. 3. Upper panel: Equipotential contour levels for the He-(1×2)Pt(110) potential drawn in the $(z, y; x = 0)$ and $(z, x; y = 3.92$ Å) planes. x, y, and z refer, respectively, to the $[1\bar{1}0]$, [001], and [110] lattice direction. The potential depth is visualized by the darkness of the shaded area. The contour lines represent the equipotential levels of -14, -10, -8, -6, -4, 0, 20, 30, 100, and 1000 (this level only in zy plane) meV, respectively. Lower panel: Maps of surface electron density in the same planes of the upper panel. The contour lines correspond, respectively (from right to left), to the electron densities of 10^{-5}, 5×10^{-5}, 1.7×10^{-4}, 6.7×10^{-4}, 1.7×10^{-3}, 3.3×10^{-3}, and 3.3×10^{-2}, 0.33 (the last two levels only in zy plane) electrons Å^{-3}.

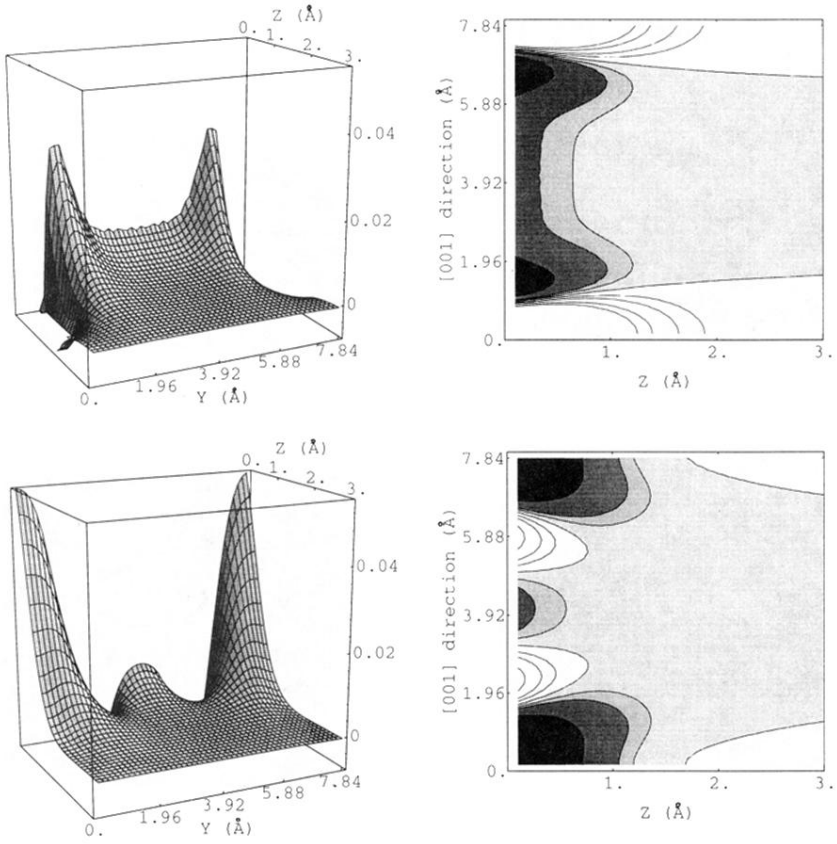

FIG. 5. Difference, $\Delta n(z, y; x = \text{const})$, between the superposition of pseudoatomic electron densities $n(\mathbf{r})$ for $\eta_x = \eta_y = 0.78$ and the superposition of free atomic densities $n(r)$, presented in the 3D figure (left-hand side) and the corresponding yz contour plot (right-hand side). x, y, and z refer, respectively, to the $[1\bar{1}0]$, [001], and [110] lattice directions. The dashed region refers to the positive values of Δn. The planes considered in the upper and lower panels intersect the atomic rows, respectively, at the *on-top* ($x = 0$) and *on-bridge* ($x = 1.38$ Å) position.